Solid State Communications 368 (2023) 115181

Contents lists available at ScienceDirect

Solid State Communications

journal homepage: www.elsevier.com/locate/ssc

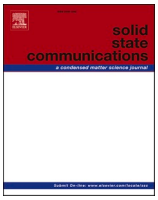

Photoionization cross-section and polarizability of impurity in CdS/ZnS core/shell quantum dots capped in a dielectric matrix

N. Zeiri [a,*], A. Cherni [a], N. Yahyaoui [a], P. Baser [b], M. Said [a], S. Saadaoui [c]

[a] Laboratory of Condensed Matter and Nanosciences (LMCN), Department of Physics, Faculty of Sciences of Monastir, 5019, Monastir, Tunisia
[b] Sivas Cumhuriyet University, Turkey
[c] Department of Physics, Faculty of Science and Arts, Mohayel Aser, King Khalid University, Abha, Saudi Arabia

ARTICLE INFO

Communicated by Asgari Reza

Keywords:
Binding energy
Photoionization cross-section
Polarizability
External electric field
Host medium

ABSTRACT

Using the effective mass approximation (E.M.A), we have performed theoretically the influence of the capped matrix, the geometrical parameters and the applied electric intensity on the Polarizability and photoionization cross-section (PCS) of CdS/ZnS core/shell quantum dots CSQDs. The energy states of the binding energy (BE) and their corresponding wave functions are computed by solving Schrödinger equation in three-dimensional based on the variational approach. Our numerical results show that the EF and the nature of dielectric medium have an obvious influence on the BE, PCS and Polarizability of the structure. The present study suggests that the c/s nanostructure dispersed in a dielectric matrix may improve the performance of optoelectronic and photonic devices.

1. Introduction

Nowadays, the low dimensionality systems such as, quantum wells (QWs), quantum wires (QW) and quantum dots (QDs) are widespread interest due to their provocative applications like tunable physical, chemical, optical and biological properties is gaining much attention among researchers [1–6]. The developments of growth techniques experimental show c/s nanostructures with different shapes. Thus, there are cylindrical [7], spherical [8] and spheroidal [9] shapes of c/s nanostructures. In this context, the c/s structures have attracted the attention of the majority of researchers due to their potential applications in the field of photonics, optoelectronics and biology [10–13]. In the biological field, nowadays a few researchers have addressed the issue on some disease and virus detection like the cancer, the coronavirus (COVID-19) and vivo tumor imaging [14,15]. However, it is indispensable to focus on the potential toxicity in the biological environment by the leakage of metal ions, which reduce the usage of QDs in the medical field. Generally, the capped process performed by organic and inorganic shells such as polymers, metal, metal oxides and metal chalcogenides reduce the toxic effects against biological systems [16–21]. Several studies have been focused on the c/s structures dispersed in a dielectric medium. In Ref. [22] the authors have performed theoretically the effect of dielectric mismatch on the BE, PCS and absorption spectrum of GaAs nanodot they demonstrated that the threshold energy and the magnitude of PCS can easily modulated by varying the heterostructure geometric factors of and the dielectric permittivity of their capped medium. In addition, Cherni et al. [23] have evaluated the effect of capping matrices (PVA, PMMA and SiO2) on the linear, third order nonlinear optical absorption coefficients and refractive index changes. They demonstrated that the biggest dielectric constant (case of PVA) has exhibited the biggest magnitude of computed coefficients. Substantial experimental outcomes and theoretical modeling for CSQDs embedded into various dielectrics medium are reported for optoelectronic device conceptions [24–27]. Stronger emitters with consistent fluorescence intensity have been achieved when authors of [28] have encapsulated CdSe/CdS QDs into SiO_2. High-dielectric constant oxide matrix such as HfO_2 is valuable due to its thermal and kinetic stability and sufficient conduction band offset at the interface limits acting as barrier for charge carriers [29]. Furthermore, in Refs. [22,30] the authors have performed theoretically the impact of dielectric mismatch on the BE, PCS and absorption spectrum of GaAs nanodot they demonstrated that the threshold energy and the magnitude of PCS can easily modulated by varying the heterostructure geometric factors of and the dielectric permittivity of their capped medium. The PCS of donor impurity in QDs under EF fields has been studied by L. M. Burileanu [31]. This investigation is performed theoretically under the EMA

* Corresponding author.
E-mail address: zeirinabil@gmail.com (N. Zeiri).

https://doi.org/10.1016/j.ssc.2023.115181
Received 26 March 2023; Accepted 17 April 2023
Available online 25 April 2023

show that the BE decrease with increasing EF and the PCS is modified by the variation of QDs size and external EF. Indeed, the magnitude of the increase with increasing QDs size and their resonance peak is accompanied by a red shift. Nonetheless, L. Aderras et al. [32] have investigated, using a variational calculation, the stark shift and the Polarizability of a symmetrical paraboloidal GaAs QDs embedded in glass matrix. They deduced that the Polarizability and the stark shift are tuning by the height of QDs and applied EF intensity.

The aim of the present was to study theoretically the influence of an applied EF intensity and the QDs size on the BE, PCS and Polarizability of the sallow-donor impurity located in the center of CdS/ZnS CSQDs surrounding in a D.M. In section1, the Eigen energies of the BE and their corresponding wave functions were performed using the variational calculation under the EMA within the framework of CDM presented. We have introduced in section.2 the theoretical model and the method used in our calculation. Our numerical results are discussed and presented in section.3. The conclusions are finally presented in section.4.

2. Model and method

In the present work, we have theoretically investigated the effect of applied EF intensity and QDs size on the BE, Polarizability and PCS of shallow –donor impurity located in the centre of CdS/ZnS CSQDs capped in a DM and presented Fig. 1 The EMA used for the purpose obtaining the wave functions and energy levels and dipole transition matrix of the system. Therefore, under the framework of EMA, the Schrödinger equation of the system is defined as:

$$(\widehat{H}_0 + \widehat{H'})\Psi_{n,l}(\vec{r}) = E_{n,l}(\vec{r})\Psi_{n,l}(\vec{r}) \tag{1}$$

$\widehat{H}_0$ is the Hamiltonian of the single electron confined in (CdS/ZnS) spherical QDs/Matrix without impurity and in absence of the EF, expressed as follow:

$$\widehat{H}_0 = \frac{-\hbar^2}{2m_j^*}\Delta + V_{conf}(\vec{r}) + \sum(R_s) \tag{2}$$

Where m_i^* is the effective mass of an electron in the i^{th} region and $V_i(r)$ is the electron confining potential inside c/s structure and F is the applied EF intensity. Both the confining potential $V_i(r)$ and the effective mass m_i^* depend on the structure position. The analytical expressions of $V_i(r)$ and

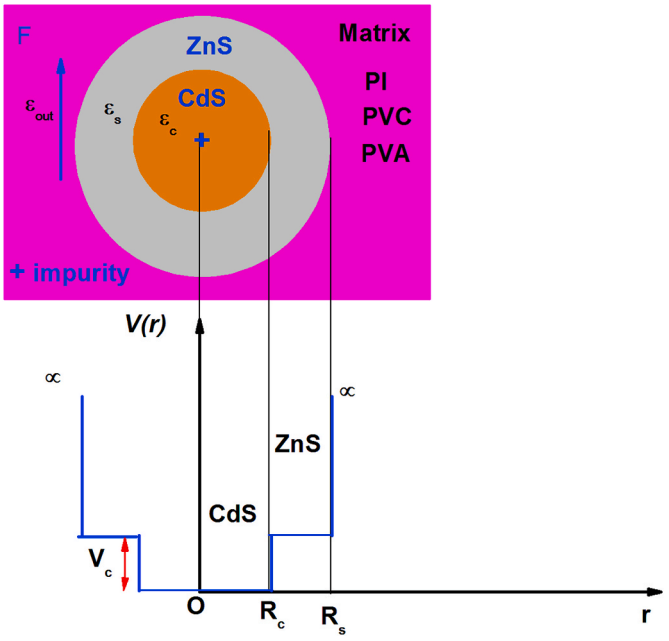

Fig. 1. Schematic plot of CdS/ZnS CSQDs immersed in three D.M.

m_i^* are defined as follow [33,34]:

$$V_i(r) = \begin{cases} 0 & 0 < r \le R_1 \\ V_c & R_1 < r \le R_2 \\ \infty & r > R_2 \end{cases} \tag{3}$$

And

$$m_i^* = \begin{cases} m_1^* & r < R_1 \\ m_2^* & R_1 < r \le R_2 \end{cases} \tag{4}$$

And $\sum(R_s)$ designate the self-polarization potential induced by the external dielectric medium, expressed as [35]:

$$\sum(R_s) = \frac{e^2}{4\pi\varepsilon_0 R_s}\left[\frac{1}{2}\left(\frac{1}{\varepsilon_{out}} - \frac{1}{\varepsilon_{in}}\right) + \frac{0.466}{\varepsilon_{in}}\left(\frac{\varepsilon_{in} - \varepsilon_{out}}{\varepsilon_{in} + \varepsilon_{out}}\right)\right] \tag{5}$$

Where $\varepsilon_{in} = \sqrt{\varepsilon_{CdS}.\varepsilon_{ZnS}}$ and ε_{out} are respectively the permittivity's of CdS/ZnS CSQDs and D.M.

In Eq. (1), $\widehat{H'}$ is considered as the perturbation Hamiltonian including the effects of Colombian potential and external EF, given by:

$$\widehat{H'} = U(\vec{r}) + eF.r.\cos(\theta) \tag{6}$$

The first term in eq (5) represent respectively, the coulomb interaction between the ion impurity and electron and between the CSQDs and DM is expressed as:

$$U_{coul}(r) = -\frac{e^2}{\varepsilon_{int} r} - \frac{e^2}{\varepsilon_{int}\varepsilon_{out} R_s}\left(\frac{\varepsilon_{int} - \varepsilon_{out}}{\varepsilon_{int} + \varepsilon_{out}}\right) \tag{7}$$

In the absence of the dielectric field and without impurity, the wave functions of $\widehat{H}_0$ can be written in spherical coordinates system as $\Psi_{n,l}^0(r,\theta,\varphi) = R_{n,l}^0(r).Y_{l,m}(\theta,\varphi)$, with $Y_{l,m}(\theta,\varphi)$ are the spherical harmonics and $R_{n,l}(r)$ is the radial part taken from Ref. [36]:

$$R_{n,l}^0(r) = \begin{cases} A_1 J_l(k_{nl,1}.r) & 0 \le r \le R_c \\ B_1 h_l^+(ik_{nl,1}.r) + B_2 h_l^-(ik_{nl,2}.r) & R_c \le r \le R_s \\ 0 & r \ge R_s \end{cases} \tag{8}$$

Where A_1, B_1 and B_2 represent the normalization constants can be determinate from the boundary conditions cited in Refs. [37,38].

$$\text{And } k_{nl,1} = \frac{\sqrt{2m_{CdS}^*(E_{n,l} - \sum(R_s))}}{\hbar^2}\ ;\ k_{nl,2} = \frac{\sqrt{2m_{ZnSe}^*(V_c + \sum(R_s) - E_{n,l})}}{\hbar^2}$$

The contribution of Coulomb potential and EF strength in Eq. (1) required the use of variational method to compute the impurity ground state energy. The trial function $R_{\lambda,\eta}(r)$ associate to the impurity ground state is taken from Ref. [38]:

$$R_{\lambda,\eta}(r) = R_{n,l}^0(r)e^{-\lambda r}e^{-\eta r\cos\theta} \tag{9}$$

In Eq. (8), λ and η are the variational parameters introduced to assume respectively the corrections made by the Colombian potential and the effect of the external EF. Considering the perturbation theory, the ground state energy of impurity must satisfy the following condition [39–42] with respect to λ and η:

$$E = \min_{\lambda,\eta}\frac{\langle\Psi_{n,l}(r,\theta,\varphi)|\widehat{H}|\Psi_{n,l}(r,\theta,\varphi)\rangle}{\langle\Psi_{n,l}(r,\theta,\varphi)|\Psi_{n,l}(r,\theta,\varphi)\rangle} \tag{10}$$

Where $\widehat{H}$ is the total Hamiltonian. The BE is defined as the difference energy between the ground states without and with impurity [43]:

$$E_b = E_0 - E \tag{11}$$

We define the Polarizability as follows:

$$\alpha_p = -\frac{e}{F}\left(\langle \Psi_{n,l}(r,\theta,\varphi)|r|\Psi_{n,l}(r,\theta,\varphi)\rangle_{F\neq 0} - \langle \Psi_{n,l}(r,\theta,\varphi)|r|\Psi_{n,l}(r,\theta,\varphi)\rangle\right) \quad (12)$$

The CSQDs structure is capped in a D.M and submitted to uniform EF. We assume that our nanostructure is a uniform dielectric medium with permittivity ε_{in} and immersed by the D.M with the permittivity ε_{out}. The authors in Ref. [44] have mentioned that in spherical nano-heterostructures the EF inside the dot F_d, is related to the outer via the expression:

$$F_d = \frac{3\varepsilon_{out}}{2\varepsilon_{out} + \varepsilon_{in}} \quad (13)$$

The PICS defines the probability of ionization of the electron attached to a hydrogenic impurity by the effect of external photon excitation. In this study, we considered the PCS describing the optical transition between ground states with and without impurity. The expression give PICS variation is given in the dipole approximation as [45–48]:

$$\sigma(\hbar\omega) = \left[\left(\frac{F_{eff}}{F_0}\right)^2 \frac{n_r}{\varepsilon_{in}}\right] \frac{4\pi^2}{3}\beta_{FS}\hbar\omega \sum_f |M_{if}|^2 \delta(\Delta E_{if} - \hbar\omega) \quad (14)$$

In the above equation, $n_r = \sqrt{\varepsilon_{in}}$ is the refractive index of QDs, $\hbar\omega$ represent the incident photon energy, F_{eff} and F_0 are the incident effective field and average field in the medium respectively in which the ratio $\frac{F_{eff}}{F_0}$ is taken equal 1 for the reason that it has no effect on PICS shape, $\beta_{FS} = \frac{e^2}{4\pi\varepsilon_0\hbar c}$ is the fine structure parameters, ΔE_{if} represent the difference on the energy. $M_{if} = F_d\langle \Psi_i|r|\Psi_f\rangle$ designate the dipole matrix element, Ψ_i and Ψ_f are the initial and final eigenwave functions with and without impurity givens respectively by Eq. (1) and Eq. (2) and $\delta(\Delta E_{if} - \hbar\omega)$ is the Lorentzian function given by:

$$\delta(\Delta E_{if} - \hbar\omega) = \frac{\hbar\Gamma}{\pi\left[\left(\hbar\omega - (\Delta E_{if})\right)^2 + (\hbar\Gamma)^2\right]} \quad (15)$$

Where $\Gamma = \frac{1}{\tau}$ is the hydrogenic impurity line-width.

3. Results and discussion

In this section, we compute and plot the PCS, stark shift and Polarizability of a spherical CdS/ZnS CSQDs dispersed in PI (polyimide), PVC (poly-vinyl alcool) and PVA (poly-vinyl chloride) D.M presented in Fig. 1. The physical parameters used in our calculations are listed in Table 1 and Table 2. We take the relaxation time as:

In order to display the influence of the geometric factors on the BE of a hydrogenic impurity on-center of a spherical CdS/ZnS CSQDs immersed in a DM, we have plotted in Fig. 2, the dependence of the BE for the ground state on core-to-shell radii ratio R_c/R_s. From this figure, it should be noted that the BE is strongly affected by the core size, it is increase, reaches a maximum and then decreases with raising R_c/R_s. This phenomenon it is due to an increase of the coulomb interaction between the electron and impurity and it is decrease with raising the core radius which is produce by the penetration of the electron wave function in the shell materials by the quantum and tunnelling effects. Our numerical results are similar with work done by M. Hbibi et al. [49]. On the other hand, from this figure, it can be noted that starting point of BE is not the same and the studied structure exhibits higher transition

Table 1
Adopted parameters in our simulations of the considered materials CdS and ZnS.

Materials	m^*/m_0	ε_r	Band offset (eV) CdS/ZnS
CdS	0.18 [33]	9.4 [33]	-
ZnS	0.42 [33]	8.4 [33]	0.897 [33]

Table 2
Various D.M used in this work and their dielectric constants.

D.M	Dielectric constant ε_{out}
PI	2.6 [48]
PVC	4 [48]
PVA	14 [33]

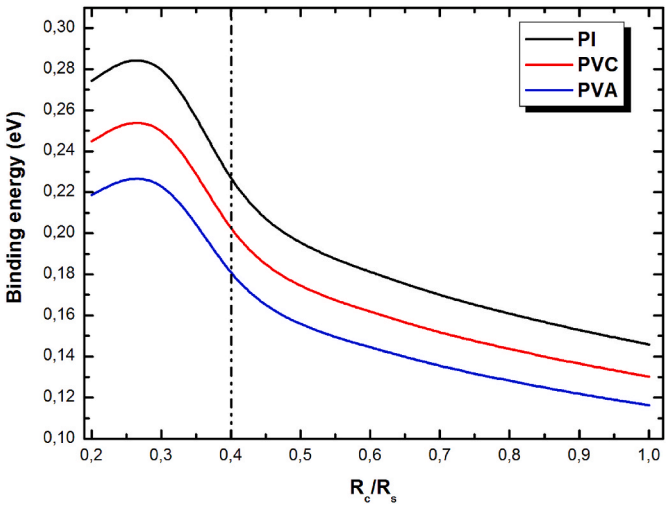

Fig. 2. The variation of ground state BE in terms of core-to-shell radii ratio R_c/R_s for three surrounding D.M.

energy in the case of the PVA matrix with permittivity $\varepsilon_{out} = 20$. Indeed, for instance with $R_c/R_s = 0.4$, $E_b = 0.227$ eV for the first matrix with permittivity $\varepsilon_{out} = 2.6$, $E_b = 0.202$ eV for the second matrix with permittivity $\varepsilon_{out} = 4$ while $E_b = 0.180$ eV for PVA matrix with permittivity $\varepsilon_{out} = 14$. Our results are in a good agreement with those mentioned in Refs. [50–52]. Adjusting the electron energy levels of QD-matrix system can offer functional engineering applications in optoelectronic devices with high quantum yield.

Fig. 3 exposed the dependence of the BE on the applied EF intensity with a fixed value of core to shell radii ratio for different D.M. From this figure, it should be noted that the BE is strongly affected by the applied EF strength, it is decrease with the raising of the applied EF strength for various D.M. This effect can be explained as: the effect of applied EF

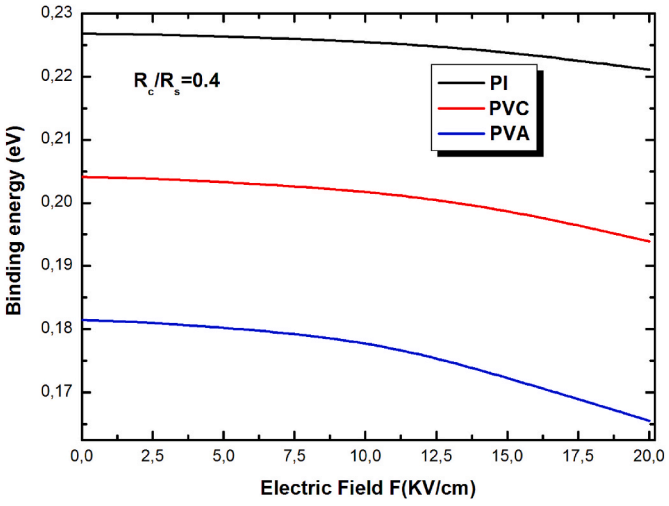

Fig. 3. The variation of ground state BE versus the applied EF strength for three surrounding D.M and for a fixed ratio $R_c/R_s = 0.4$.

intensity broken the symmetric and reinforced the asymmetric of the structure which is reduced the energy levels and therefore the BE. The same behaviour was already observed in spherical CSQDs, and qualitatively explained in Ref. [30] when the authors have studied the impact of EF on the impurity states and PCS in CdSe/ZnS c/s nanodots with dielectric confinement, they demonstrated that the effect of the applied EF produces to a raise of the electron–impurity distance, with the decreasing of the Coulomb interaction. Then, the wave function becomes more extended in the shell material where the electron has a greater effective mass compared to that in the core region. So, the decreasing behavior of the ground state energy E_1 versus EF is explained by the reduction of the kinetic energy term in the Schrödinger equation. In order to understand the contribution of the applied EF intensity on the BE, we have exposed in Fig. 4 the dependence of the stark shift on the applied EF strength for three D.M. However, the stark shift is defined as follows: the BE difference with and without applied EF intensity [41]. The calculations are performed at a fixed value of core-to-shell radius ratio $R_c/R_s = 0.4$. One can be seen from this figure that the stark shift decrease quadratically with the applied EF orientation for various D.M. We remark for PI DM with the permittivity $\varepsilon_{out} = 2.6$ the stark shift not significant with raising the applied EF strength because in this case we have a strong confinement of the electron. This effect is explained as: the electron cannot be separated apart so for due to the geometrical confinement which is strong and predominant and the coulomb potential effect is also important and the charge distribution is less sensitive to EF. Whereas for the PVA D.M with permittivity $\varepsilon_{out} = 14$ we have a weak confinement and the electron can be pulled apart so for with tunneling effect. Our computation is an excellent agreement with the work done in Ref. [41]. In Fig. 5 we have depicted the stark shift on the BE versus EF intensity for three size of the core radius in the case of PVA D.M with dielectric constant $\varepsilon_{out} = 14$. It is easy to found that the stark shift not only affected by EF but also by the QDs size. One can see from this figure that the stark shift has a parabolic behavior which increases with increasing the QDs size. On the other hand, for the smallest QDs size, the Stark shift has almost a linear behavior. Our finding is an excellent agreement with the work done in Ref. [50].

According to eq (6) we have tested the effect of the geometric parameters on the Polarizability presented in Fig. 6 for three surrounding D.M with a fixed value of EF at 5 kV/cm. From this figure, it can be seen that the Polarizability is strongly affected by the QDs size. It is increase with increasing the QDs size of the structure. This result is predictable because for a large value of R_c/R_s we have a weaker confinement. Our numerical results are similar to that observed in QDs and QWW [51]. Moreover one can be seen form the figure that the capped matrix which

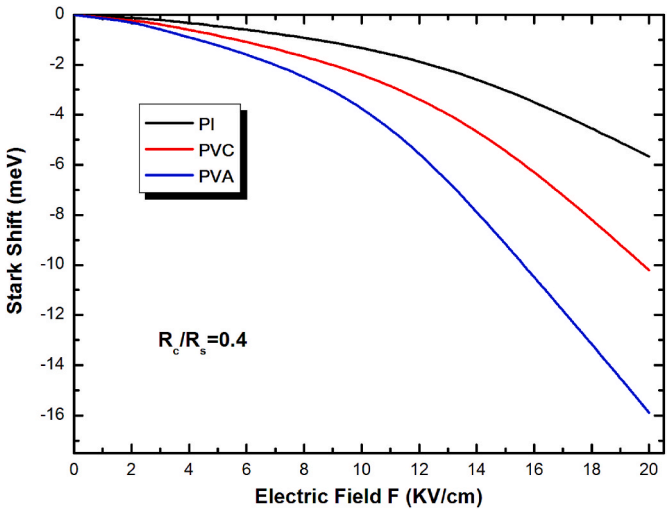

Fig. 4. The variation of the Stark-shift versus EF strength for three surrounding D.M and for a fixed ratio $R_c/R_s = 0.4$.

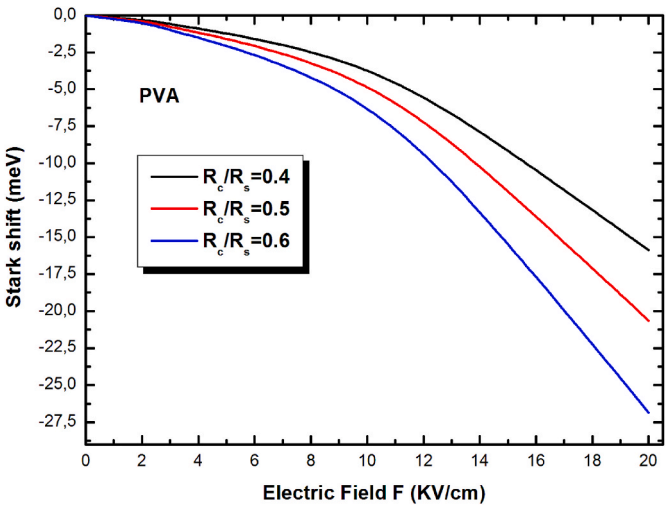

Fig. 5. The dependence of the Stark-shift on the EF strength for different core radius in the case of PVA matrix.

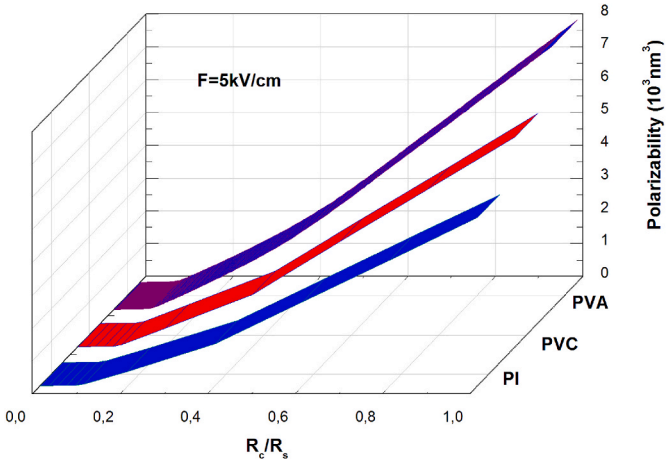

Fig. 6. The dependence of the Polarizability on the core to shell radius ratio R_c/R_s for three surrounding D.M under condition F = 5 kV/cm.

have a higher dielectric constant exhibit a strong Polarizability, while the immersed matrix which has a lower dielectric constant exhibit a weaker Polarizability. These results are in good concordance to that presented in Refs. [52,53]. When the authors have studied theoretically the impact of dielectric medium in the optical properties they showed that the QD dispersed in a matrix having a higher D.M exhibit an improvement of the absorption peak intensity, whereas when the QD immersed in a matrix having a lower D.M exhibit a weaker absorption peak intensity. Furthermore, the influence of the applied EF on the PCS of the impurity ions is shown in Fig. 7. It is easy to observe from this figure that the Polarizability decrease with increasing the EF intensity and, it is stronger in the case of PVA matrix.

In order to improve the performance of the optoelectronic device, we have depicted in Fig. 8 the variation of the PCS versus incident photon energy for three capped D.M, for a fixed value of radius ratio $R_c/R_s = 0.4$ under condition F = 0 kV/cm. From this figure it can be seen that the PCS increase and their resonance peak intensity move to lower energies. This shift can be explained as follows: Here, two cases may be arise: when we deal with the PI matrix, in this case we have $\varepsilon_{in} > \varepsilon_{out}$ and the local field factor $F < 1$ which is induced a weaker PCS, when we deal with the PVA matrix, in this case we have, $\varepsilon_{in} < \varepsilon_{out}$ and the local field factor $F > 1$ resulting in an increase of the transition matrix element giving a stronger PCS. The same conclusion has been established by Zeng

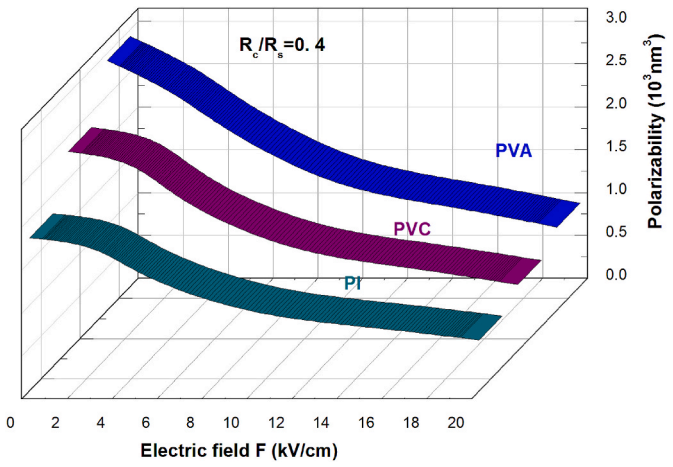

Fig. 7. The dependence of the Polarizability on the FE strength for a fixed value of core to shell radius ratio $R_c/R_s = 0.4$ in the case PVA matrix.

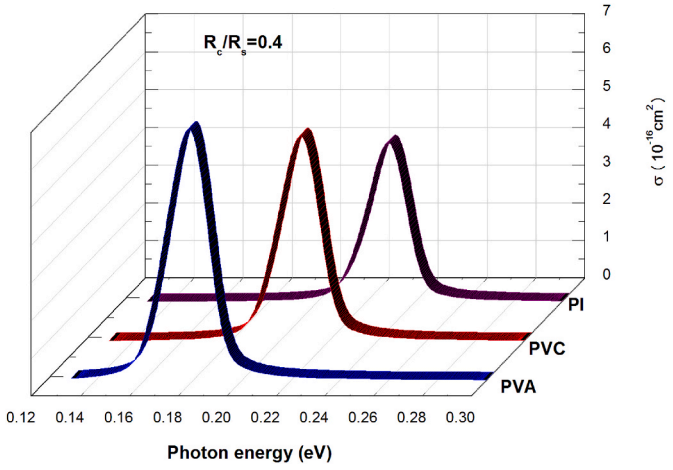

Fig. 8. The PICS variation in terms of incident energy photon for different values of core to shell radius ratio R_c/R_s in the case PVA matrix.

et al. [54]. In other word, we can say that PCS dependency analysis can be explored to identify the optimal geometric parameters as well as suitable host material of nanostructure layers to realize the photonic and optoelectronic devices.

Finally, in order to investigated the influence of the EF on the optical properties, the variation of the PCS in terms of photon energy for the PVA matrix and for a fixed value of the radius ration R_c/R_s is computed and shown in Fig. 9. From this figure, it should be noted that the PCS peak intensity increase with raising the applied EF intensity and their resonance peaks toward to lower energies. This result is expected because the impact of EF strength on CdS/ZnS structure broken the symmetry and can only reinforce the asymmetry. In this case the energy difference decrease with increasing the EF intensity and there is an improvement of the dipole matrix which exhibit an enhancement of the PCS intensity. It is clear on this figure to see that the PCS reaches a maximum for F = 20 kV/cm. We have proved that the PCS can be controlled with modifying the applied electric strength, the D.M and the geometrical factors. These properties can be useful for producing some device applications such as QD infrared photo detectors.

4. Conclusions

In this paper, we have performed a theoretical investigation on the BE of a hydrogenic impurity, the PCS and stark shift CdS/ZnS c/s QDs

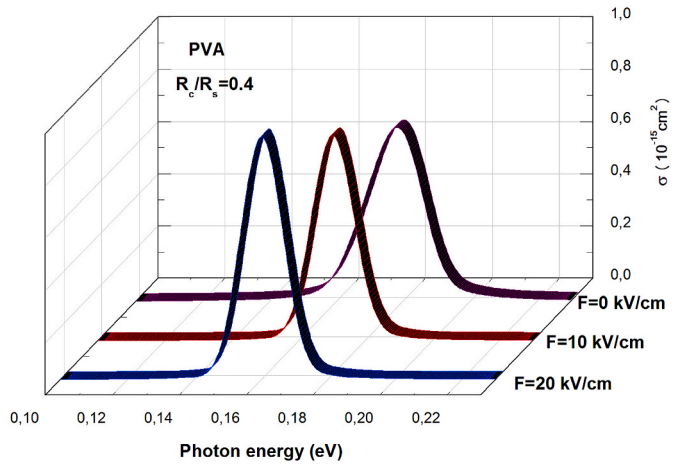

Fig. 9. The PICS variation in terms of incident energy photon for different EF strengths in for a fixed core radius $R_c = 0.4R_s$ and in the case the case PVA matrix.

embedded in three D.M under the E.M.A with the presence of applied EF strength. The results revealed that the electron wave function is more compressed and localized when CSQD embedded into lower dielectric medium. The dielectric confinement should be explored to adjust the resonant energies. Our results indicated that controlling the inner CdS core provides an efficient confinement of electron. With large PCS our model has come out as a promising candidate for the manufacture of optoelectronic and photonic devices.

Declaration of competing interest

The authors declare that they have no known competing financial interests or personal relationships that could have appeared to influence the work reported in this paper.

Data availability

No data was used for the research described in the article.

Acknowledgements

The authors extend their appreciation to the Deanship of Scientific Research at King Khaled University for funding this work through large group Research Project under grant number RGP2/19/44.

References

[1] P. Hawrylak, Phys. Rev. B 60 (1999) 5597–5608.
[2] H.H.-Y. Wei, C.M. Evans, B.D. Swartz, A.J. Neukirch, J. Young, O.V. Prezhdo, T. D. Krauss, Nano Lett. 12 (2012) 4465–4471.
[3] Y.-P. Gu, R. Cui, Z.-L. Zhang, Z.-X. Xie, D.-W. Pang, J. Am. Chem. Soc. 134 (2012) 79–82.
[4] K. Dohnalová, A.N. Poddubny, A.A. Prokofiev, W.D. de Boer, C.P. Umesh, J. M. Paulusse, H. Zuilhof, T. Gregorkiewicz, Light Sci. Appl. 2 (2013) e47, e47.
[5] S. Jin, Y. Hu, Z. Gu, L. Liu, H.-C. Wu, 2011 (2011) 1–13.
[6] S.J. Rosenthal, J.C. Chang, O. Kovtun, J.R. McBride, I.D. Tomlinson, Chem. Biol. 18 (2011) 10–24.
[7] F. Ungan, M.K. Bahar, M.G. Barseghyan, L.M. Pérez, D. Laroze, Optik 236 (2021), 166621(1)-166621(7).
[8] L. Máthé, C.P. Onyenegecha, A.-A. Farcaş, L.-M. Pioraş-Ţimbolmaş, M. Solaimani, H. Hassanabadi, Phys. Lett. 397 (2021), 127262(1)-127262(10).
[9] A.A. Gusev, O. Chuluunbaatar, L.L. Hai, S.I. Vinitsky, E.M. Kazaryan, H. A. Sarkisyan, V.L. Derbov, J. Phys. Conf. Ser. 393 (2012), 012011(1)-012011(9).
[10] J. Kim, S. Song, Y.-H. Kim, S.K. Park, Small Struct 2 (2021), 2000024.
[11] E. Stokes, A.D. Stiff-Roberts, C.T. Dameron, Electrochem. Soc. Interface 15 (2006) 23.
[12] R.E. Bailey, A.M. Smith, S. Nie, Syst. Nanostructures. 25 (2004) 1–12.
[13] J. Shen, Y. Zhu, X. Yang, C. Li, Chem. Commun. 48 (2012) 3686–3699.
[14] S.R. Ahmed, S.W. Kang, S. Oh, J. Lee, S. Neethirajan, Heliyon 4 (2018), e00766.

[15] J. Gao, K. Chen, R. Xie, J. Xie, S. Lee, Z. Cheng, X. Peng, X. Chen, Small 6 (2010) 256–261.
[16] J. Mal, Y.V. Nancharaiah, E.D. van Hullebusch, P.N.L. Lens, RSC Adv. 6 (2016) 41477–41495.
[17] S. Stankic, S. Suman, F. Haque, J. Vidic, J. Nanobiotechnol. 14 (2016), 73(1)-73 (20).
[18] A.A. Yaqoob, H. Ahmad, T. Parveen, A. Ahmad, M. Oves, I.M.I. Ismail, H.A. Qari, K. Umar, M.N. Mohamad Ibrahim, Front. Chem. 8 (2020) 1–23.
[19] A. Mustafai, M. Zubair, A. Hussain, A. Ullah, Polymers 15 (2023) 836.
[20] J. Kaur, V. Mishra, S.K. Singh, M. Gulati, B. Kapoor, D.K. Chellappan, G. Gupta, H. Dureja, K. Anand, K. Dua, G.L. Khatik, K. Gowthamarajan, J. Contr. Release 334 (2021) 64–95.
[21] S. Movassaghian, O.M. Merkel, V.P. Torchilin, WIREs Nanomedicine Nanobiotechnology 7 (2015) 691–707.
[22] E.C. Niculescu, Opt Commun. 284 (2011) 3298–3303.
[23] A. Cherni, N. Zeiri, N. Yahyaoui, M. Said, Chem. Phys. 539 (2020), 110947.
[24] K.H. Ibnaouf, S. Prasad, M.S. Al Salhi, A. Hamdan, M.B. Zaman, L. El Mir, J. Lumin. 149 (2014) 369–373.
[25] R. Tan, Y. Shen, S.K. Roberts, M.Y. Gee, D.A. Blom, A.B. Greytak, Chem. Mater. 27 (21) (2015) 7468–7480.
[26] A. Ibral, A. Zouitine, S. Aazou, E.M. Assaid, E.M. Feddi, F. Dujardin, J. Optoelectron. Adv. Mater. 15 (11–12) (2013) 1268–1274.
[27] J.M. Gordon, Y.N. Gartstein, JOSA B 31 (9) (2014) 2029–2035.
[28] B.D. Anderson, W.C. Wu, J.B. Tracy, Chem. Mater. 28 (14) (2016) 4945–4952.
[29] C. Palade, A. Slav, O. Cojocaru, V.S. Teodorescu, T. Stoica, M.L. Ciurea, A.M. Lepadatu, 12(3), (2022) 348-352.
[30] E.C. Niculescu, M. Cristea, J. Lumin. 135 (2013) 120–127.
[31] L.M. Burileanu, J. Lumin. 145 (2014) 684–689.
[32] L. Aderras, A. Bah, E. Feddi, F. Dujardin, C.A. Duque, Phys. E Low-Dimens. Syst. Nanostructures. 89 (2017) 119–123.
[33] N. Zeiri, A. Naifar, S. Abdi-Ben Nasrallah, M. Said, Results Phys. 15 (2019), 102661.
[34] K. Hasanirokh, A. Asgari, M. Mahdizadeh Rokhi, Optik 188 (2019) 99–103.
[35] Anchala, S.P. Purohit, K.C. Mathur, J. Appl. Phys. 110 (2011), 114320(1)-114320 (8).
[36] T.O. Cheche, V. Barna, Y.-C. Chang, Superlattice. Microst. 60 (2013) 475–486.
[37] L. Shi, Z.W. Yan, Superlattice. Microst. 94 (2016) 204–214.
[38] S. M'zerd, M. El Haouari, M. Aghoutane, M. El-Yadri, E. Feddi, F. Dujardin, I. Zorkani, A. Jorio, M. Sadoqi, G. Long, J. Appl. Phys. 124 (2018), 164303(1)-164303(8).
[39] L. Shi, Z.W. Yan, Superlattice. Microst. 94 (2016) 204–214.
[40] D.A. Baghdasaryan, E.M. Kazaryan, H.A. Sarkisyan, Superlattice. Microst. 104 (2017) 69–77.
[41] L. Aderras, A. Bah, E. Feddi, F. Dujardin, C.A. Duque, Phys. E Low-Dimens. Syst. Nanostructures. 89 (2017) 119–123.
[42] A.L. Morales, N. Raigoza, E. Reyes-Gómez, J.M. Osorio-Guillén, C.A. Duque, Superlattice. Microst. 45 (2009) 590–597.
[43] D. Maikhuri, S.P. Purohit, K.C. Mathur, AIP Adv. 2 (2012), 012160(1)-012160(14).
[44] H. Baghramyan, M. Barseghyan, A.A. Kirakosyan, R. Restrepo Arango, M. Mora-Ramos, C. Duque, J. Lumin. 145 (2014) 676–683.
[45] M.G. Barseghyan, M.E. Mora-Ramos, C.A. Duque, Eur. Phys. J. B 84 (2011) 265–271.
[46] K. Rahmani, Y. Chrafih, S. M'Zred, S. Janati, I. Zorkani, A. Jorio, A. Mmadi, J. Phys. Conf. Ser. 984 (2018), 012001(1)-012001(8).
[47] A.L. Morales, N. Raigoza, E. Reyes-Gómez, J.M. Osorio-Guillén, C.A. Duque, Superlattice. Microst. 45 (2009) 590–597.
[48] Brijesh Kumar, Brajesh Kumar Kaushik, Y.S. Negi, J. Mater. Sci. Mater. Electron. 25 (2014) 30.
[49] M. Hbibi, O. Mommadi, S. Chouef, R. Boussetta, L. Belamkadem, A. El Moussaouy, F. Falyouni, C.M. Duque, J.A. Vinasco, C.A. Duque, Scientific report 14854 (2022) 1–19.
[50] A. Chafai, F. Dujardin, I. Essaoudi, A. Ainane, R. Ahuja, Superlattices and Microstructures vol. 111, 2017, pp. 976–982.
[51] M. Elamathi, A. John Peter, C.W. Lee, the European Physical Journal D 74 (2020) 196.
[52] Z. Zeng, C.S. Garoufalis, S. Baskoutas, A.F. Terzis, Phys. Lett. 376 (2012) 2712–2716.
[53] S.M. Martina, B. Sukumar, Solid State Commun. 85 (1993) 623–723.
[54] Z. Zeng, C.S. Garoufalis, S. Baskoutas, A.F. Terzis, Journal of electronics and Optoelectronics 11 (2016) 1–5.